OPEN ACCESS

Time-Efficient Reparameterization and Simulation of Manufacturing Impacts on Performance of Lithium-Ion-Batteries

Time-Efficient Reparameterization and Simulation of Manufacturing Impacts on Performance of Lithium-Ion-Batteries

Georg Lenze,[1,2] Vincent Laue,[1,2] and Ulrike Krewer[1,2,z]

[1] *Institute of Energy and Process Systems Engineering, TU Braunschweig, 38106 Braunschweig, Germany*
[2] *Battery LabFactory Braunschweig, 38106 Braunschweig, Germany*

The high quality demands of batteries for electric vehicles require powerful tools for error detection in cell manufacturing. Furthermore, cell diagnostics is a serious challenge because performance limitations occur on atomic scale and as batteries are closed systems physical issues can hardly be detected only with the aid of experimental methods. Physico-chemical models enable to detect up to seven various mechanisms of limitations but experimental parameterization is extensive. Therefore, in this study a fast mathematical parameterization approach was used to simulate and diagnose cells with various manufacturing parameter configurations. Limitation mechanisms are shown in correlation with impacts by calendering, electrode thickness, carbon black recipe and cathode active material. Depending on the adjusted production parameters, they vary between low electronic conductivity, overpotentials due to reduction of electrochemically active solid-liquid interfacial area and low ionic conductivity. Furthermore it is shown that characteristic indicators for the particular limitation mechanisms can be observed in discharge curves at various C-Rates. Finally, a statistical analysis demonstrates how parameter identification can be performed computationally as a side product from reparameterization.
 [DOI: 10.1149/2.0751913jes]

Manuscript submitted March 29, 2019; revised manuscript received July 8, 2019. Published August 27, 2019.

Batteries are the bottleneck for the development and breakthrough of electromobility. To improve battery performance, it is essential to understand the cell internal physico-chemical behavior and its correlation with manufacturing parameters. After assembly the battery cells are closed systems which makes it difficult to place sensors inside and to investigate correlations experimentally during discharge.[1] In view of the e-mobility-driven demand for ever more powerful battery cells, the further development of diagnostic technologies is of high relevance. Due to the black box problem and the physical interactions on very small scales between molecule and micro meter level, there are numerous error mechanisms, the complexity of which becomes apparent in investigations both on conventional lithium-ion-cells[2,3] and on next generation technologies such as the all solid state battery.[4,5] Physico-chemical battery models are powerful tools for in-depth diagnosis because the simulation does not only save material costs and measurement time but it also enables to study cell internal processes like diffusion, reaction kinetics, electronic and ionic conduction.[6–9] The high significance of the simulation in the context of typical challenges from the automotive sector is shown e.g. within the study of Campbell et al.[10] which adresses the requirement of reconciling high driving range with fast charging capability.

Unfortunately model parameterization is time and cost extensive and has to be repeated for each individual cell. Ecker et al. show in their studies about parameterization several experiments and evaluation methods which are required.[11,12] Another challenge to make physico-chemical models suitable for industrial applications is that several of the parameters are difficult or not feasible to measure in general and that results from various sources in literature deviate strongly from each others. E.g. Ecker et al. and Park et al. reviewed different sources and revealed that electronic conductivities and diffusion coefficients of electrode materials varied by several orders of magnitude.[11,13] About electrode tortuosities, Thorat et al. summarized the results of several studies which deviate from each other as well.[14] Ott et al. presented a novel approach on tortuosity determination which assumes that the tortuosity is effectively even higher than estimated in many studies because inhomogeneities of pore diameters are usually not considered.[15] An alternative strategy for model parameterization which is promising to reduce the effort, is to identify most or even all parameters by computational fitting.[16,17] Such model-based parameter identification using discharge curves of real cells at different C-Rates promises quite reliable parameter sets because the current dependent discharge curves offer particular properties which are unique for each individual cell, e.g. curve shape and distances of the curves to each other.[18] Alternative approaches are fitting of equivalent circuits to electrochemical impedance spectra.

However such gray or black box models do not give physical insight into the cell and they are not useful to interpret the omnipresent C-Rate tests also.[19] Physico-chemical models which reproduce impedance as well as discharge curves are still lacking for batteries while scarcely being available for fuel cells.[20] Similarly, several data-driven state of charge (SOC) and state of health (SOH) estimation processes exist, but also they do not allow a physical insight into the processes. They though might be trained to identify such errors via data mining.[19] Development of a time saving parameterization strategy is important to make physico-chemical simulation attractive for industrial applications. Extensive experimental parameterization strategies appear to be a main issue hindering physico-chemical models to become an economically efficient tool in battery mass production. The ability to identify the cell internal limiting process without spending time and production costs for test cells would significantly improve battery diagnostics and thereby also battery costs.

From the previous work[1] where model parameterization was performed in a fundamental research perspective with extensive experimental parameter identification it is visible that there is a lack of connectivity between research and application oriented feasibility. In this work a physico-chemical model with given parameter set from previous investigations was mathematically reparameterized with the aim to improve the previous approach by making it more time efficient and therefore economically more helpful for usability in industrial battery production. Furthermore this study should create additional methods for the complex field of cell diagnosis which is limited due to the difficult situation of cells being closed black box systems. After validation with experimental results the model was used to analyze several manufacturing parameter impacts. Reduced effort by numerical reparameterization is shown to enabled to simulate various, typical manufacturing impacts. For all impacts, the dominant cell internal performance limiting processes are shown. Then all derived parameter sets were statistically analyzed for comparison for future parameterization of battery models as reference.

Experimental

Electrodes and battery cells.—This study is based on experimental data from previously characterized electrodes.[21] Based on these measurements and material densities ρ_i, the respective electrode porosities ε and solid volume fractions of active material ε^s_{act} and

[z] E-mail: u.krewer@tu-braunschweig.de

inactive additives ε^s_{add} such as carbon black and binder were calculated as described in Lenze et al.[1] according to the equations:

$$\varepsilon^s_{act} = \frac{\varpi}{\delta} \cdot \frac{\zeta_{act}}{\rho_{act}} \quad [1]$$

$$\varepsilon^s_{add} = \frac{\varpi}{\delta} \cdot \frac{\zeta_{add}}{\rho_{add}} \quad [2]$$

$$\varepsilon = 1 - \varepsilon^s_{act} - \varepsilon^s_{add} \quad [3]$$

with electrode material loading ϖ, electrode thickness δ and mass fraction ζ. The single-layered pouch cells used in the previous study[21] had an electrode surface area of 24.95 cm^2 and C_6 (graphite) anodes, calendered to 10 % volume reduction. CELGARD2320 separator and a solution consisting of 3:7 EC:DEC, 1 M $LiPF_6$ was used as electrolyte.

For the cathodes several production parameters were varied:

1) non-calendered vs. 22 % calendered,
2) electrode thickness of NMC 48.95 µm vs. 61.49 µm,
3) carbon black (CB) content and carbon black to binder ratio (CB:B) with CB 4 mass-%, CB:B = 1 vs. CB 5.88 mass-%, CB:B = 1.5,
4) active material $Li(Ni_{1/3}Mn_{1/3}Co_{1/3})O_2$ (NMC) vs. $LiMn_2O_4$ (LMO).

The four configurations of parameter variations listed here are also referred to in the following as production impacts and are described in detail with regard to their respective effects on the parameter set in the Table AI in the Appendix. The electrodes with low thicknesses had a theoretical area capacity of 1.40 mAh cm^{-2} and the ones with increased thickness had a theoretical area capacity of 1.85 mAh cm^{-2}. This value is composed of the mass related intrinsic capacity which is given in the data sheet of the active material and of the set parameters in electrode production, i.e. the mass fraction of the active material within the slurry and the weight per unit area during coating. The theoretical cell capacities were calculated on the basis of the theoretical area capacity and the electrode area surface of the pouch cells used here to 24.95 $cm^2 \cdot 1.40$ mAh $cm^{-2} = 34.93$ mAh for the reference cell (see Table I) as well as for cells (a) and (c) with thin electrodes δ and to 24.95 $cm^2 \cdot 1.85$ mAh $cm^{-2} = 46.16$ mAh for the cells (b) and (d) with increased δ according to Table AI, respectively. However, since the real discharge capacities from the formation were in some cases significantly lower than the theoretical values, the currents for the C-rate tests were recalculated on the basis of the capacity measured in the second discharge step of the formation. Accordingly, the determined real capacities were for the reference cell: 31.74 mAh and concerning the cells according to Table AI for cell a: 32.06 mAh, cell b: 40.72 mAh, cell c: 32.40 and cell d: 38.98 mAh. As LMO has a lower capacity of lithium which can be intercalated per volume element than NMC, the cells with LMO cathodes have a larger layer thickness than those with NMC to realize the same cell capacity. The layer thickness of the LMO cathode in cell d was 86.96 µm accordingly. Details of formation and measurement routines are the same as described in our previous study.[21] For evaluation of cell performance, discharge curves at 0.2C, 0.5C, 1C, 2C and 5C were used within a range of cut-off-voltages of 2.9 V and 4.2 V. As LMO has a lower capacity of lithium which can be intercalated per volume element than NMC, the cells with LMO cathodes have a larger layer thickness than those with NMC to realize the same cell capacity. The layer thickness of the LMO cathode in cell d was 86.96 µm accordingly.

Physico-chemical model and parameterization.—For simulation-supported battery analysis, we used a pseudo 2-dimensional (P2D) physico-chemical battery model based on the work of Legrand et al.[7] with slight modifications which were presented in previous work[1] in detail. Therefore in this study there will be only a short description be given. As shown in Figure 1, the model was discretized in the direction perpendicular through the cell and also the active material particles of anode and cathode were discretized in radial direction. The governing equations account for Fick's diffusion of lithium in the solid particles and in the liquid electrolyte. Charge transport of electrons in the electrodes and of lithium ions in the electrolyte are considered by Ohm's law. To describe the electrochemical reaction kinetics in anode and cathode, respectively, the Butler-Volmer equation was implemented; it also includes the solid-liquid interfacial area a_{sl} which can effectively deviate from the theoretically available surface area of the particles when e.g. due to poor electronic connection with the carbon black binder matrix parts of the interfacial area become isolated.[1,22] As a reference, the parameter set for a cell with non-calendered NMC cathode was taken which was derived in previous work[1] by a combination of measurements, literature research and fitting. It is shown in Table I, first column. For this work, the model was reparameterized by determining all parameters numerically by least square approximation to optimal agreement between simulation and real cell behavior and to compare results of both parameterization strategies. Parameterization by numerical calculation is attractive due to significant reduction of effort. Therefore it was then applied to the four other electrode configurations representing the four manufacturing impacts, respectively, which were introduced in Electrodes and battery cells subsection and depicted in Table AI. The aim was to test the general functionality of this parameterization approach for cell diagnosis in battery production plants. To reproduce the open circuit potential of LMO, a simplified polynomial was derived which corresponds to the half cell discharge behavior at 0.1C given by the active material manufacturer in the material data sheet. This polynomial is a function of lithium concentration $\bar{c}$ within the LMO particles and given by the equation:

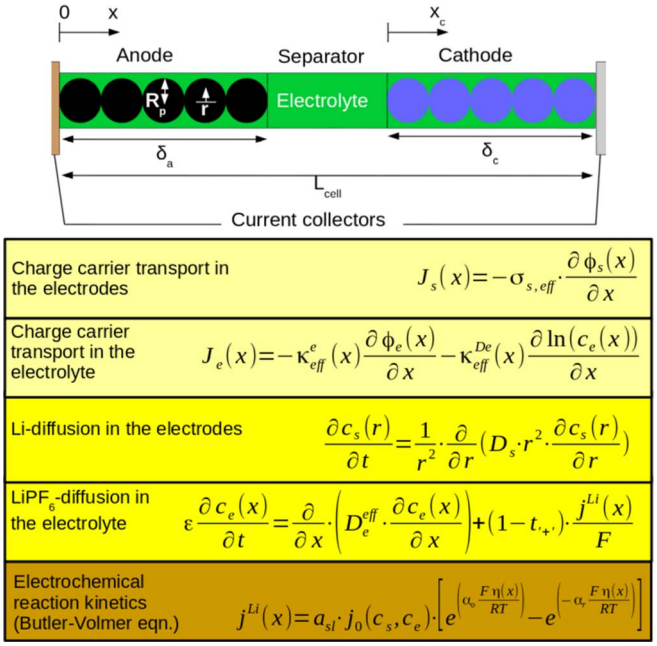

Figure 1. Summary of the P2D physico-chemical battery model[1] which is discretized over particle radii and cell length; the governing equations include Ohm's conduction, diffusion and reaction kinetics.

$$U = \frac{-4997 \cdot \bar{c}^2 - 645.9 \cdot \bar{c} + 5685}{\bar{c}^4 - 36.23 \cdot \bar{c}^3 - 1318 \cdot \bar{c}^2 + 29.47 \cdot \bar{c} + 1337} \quad [4]$$

where $\bar{c}$ is given by the dimensionless quotient of lithium concentration at a particular state of charge c_c and the maximum concentration intercalatable into the active material c_c^{max}:

$$\bar{c} = \frac{c_c}{c_c^{max}} \quad [5]$$

In the model, the lower Li intercalation capacity of the LMO described above was taken into account by the different c_c^{max}-values for both cathode materials in addition to the different layer thicknesses. Accordingly, for LMO[18] $c_c^{max,LMO} = 15120$ mol m^{-3} and for NMC[1] $c_c^{max,NMC} = 49244$ mol m^{-3} was implemented. For comparison of the

various parameter configurations and their impacts to each other in the results section, the respectively best performing out of the four cells manufactured per configuration was taken. The only exception is the reference example with the cell with non-calendered cathode discussed in Assessment of numerical parameterization subsection where performance mean values out of four equivalent cells were taken just as in Lenze et al.[1] In this case it was the main priority to make both parameter sets, the one derived from literature and experiments[1] and the one recalculated by fitting, comparable to each others.

Optimization algorithm.—For simulation-based parameter estimation, a least square curve fitting routine was applied. As initial values the parameters of the non-calendered reference case were taken. It is based on a trust-region-reflective algorithm which is already implemented in Matlab. The least square problem is defined as follows:

$$X^* : F(X^*) = \min_{X \in \mathbb{R}^N} |F(X)| \qquad [6a]$$

$$F(X) = \sum_{j}^{m} \left(\sum_{k=1}^{n} \left(U_{\text{sim}}(C_k, X, t) - U_{\text{exp}}(C_k, t) \right)^2 / U^2_{\text{max},j} + \sum_{k=1}^{n} \left(C_{\text{sim}}(U_k, X) - C_{\text{exp}}(U_k) \right)^2 / C^2_{\text{max},j} \right) \qquad [6b]$$

The algorithm with X being the parameters and X^* the identified parameter values, adjusts the parameters to reproduce the experimental C-rate test for all C-rates, simultaneously. Simulated capacity C_{sim} and cell voltage U_{sim} are compared with the experimental capacity C_{exp} and cell voltage U_{exp} for equidistant interpolation points C_k and U_k, respectively. Both deviations are normalized to the maximum capacity C_{max} or voltage U_{max}, respectively.

Simulation-supported cell diagnosis.—A promising benefit of physico-chemical models is that cell internal processes during discharge can be simulated. This enables to identify the particular processes in malfunctioning cells which limit the performance. Figure 2 depicts the different limiting processes and how characteristic performance limitations can be attributed to them. Limitations due to electrode overpotentials, electronic conduction and diffusion in the solid active material can separately be evaluated for anode and cathode, which yields six different limitation cases. The ionic conduction in the electrolyte is balanced over the entire cell, yielding seven cases in total. The concentrations are plotted over the normalized lengths of particles, electrodes and cell, respectively. In the case of particle concentration the x-axis represents the particle radius where the point in the middle of the particle is at 0 and the particle surface at 1 on the x-axis. Normalization over the anode is depicted with the boundary to current collector at 0 and boundary to separator at 1 on the x-axis, for the cathode this is vice versa. The concentration of $LiPF_6$ in the electrolyte is plotted over the normalized cell length where 0 on the x-axis represents the boundary between anode and current collector and 1 is the boundary between cathode and current collector. Case 1 and 2 in Figure 2 show a performance limitation during discharge in the diffusion of lithium within the particles of anode and cathode respectively, where the solid concentration is plotted over the normalized particle radius. In the anode, before discharge starts, the lithium concentration is on a high, saturated level c_a^0. When limitation occurs during discharge, as shown in case 2, the concentration in the particle center may still be close or even equal to c_a^0. However, due to poor diffusion a large concentration gradient over the particle radius develops so that at the particle surface lithium can not be supplied fast enough which results in a depletion, indicated by concentration becoming equal to zero in the related diagram in Figure 2. Case 2 shows limitation by solid diffusion in the cathode. The curve shape is similar as for the anode but it is vice versa in terms of a low concentration level before discharge starts. As the concentration increases during discharge, cathodic limitation occurs if the curve approaches the maximum intercalatable concentration $c_c^{\max}$. In this case the concentration gradient indicates that due to poor diffusion the lithium cannot be transported fast enough to the center of the particle where the concentration may still be low, whereas at the particle surface with $c_c^{\max}$ a saturation is reached already so that no further lithium can be intercalated. Analogously the same indicators, meaning anodic concentrations approach zero and cathodic concentrations approach $c_c^{\max}$, respectively, are valid in cases 3 and 4 for identification of limitation by poor electronic conductivity. However, characteristic for limitation by conductivity is that the dominant concentration gradient is not the one between particle center and surface but the one over the normalized electrode length. It results from a depletion of electrons at the respective location where the electrons have the longest transportation pathway which is at the border between current collector and electrode for anode and the border between electrode and separator for cathode. Case 5 depicts a performance limitation by poor ionic conductivity in the electrolyte which is caused by a large gradient of $LiPF_6$ concentration along the cell length. It approaches zero in the cathode where the too slow transportation of ions yields a depletion of intercalatable lithium. Not only poor ionic conductivity of the electrolyte but also a too high tortuosity of the electrodes can lead to this kind of limitation. Cases 6 and 7 can be comprised in one diagram. These cases depict limitations due to poor electrochemical reaction kinetics at the interface between particles and electrolyte which can either be caused by a low reaction rate constant or by an effectively decreased solid-liquid interfacial area. These performance losses are considered by overpotentials η calculated by Butler-Volmer equations for anode and cathode, respectively. Overpotentials can directly be observed in discharge curves derived by C-Rate tests in terms of a drop of cell voltage. In the application of the overpotentials from anode η_a and cathode η_c in one diagram the total overpotential η results from

$$\eta = \eta_a + |-\eta_c| \qquad [7]$$

which then has to be subtracted from the cell OCV to quantify the performance loss. Whether the overpotential from anode or cathode has a limiting effect is determined by the higher absolute value of η_a or η_c.

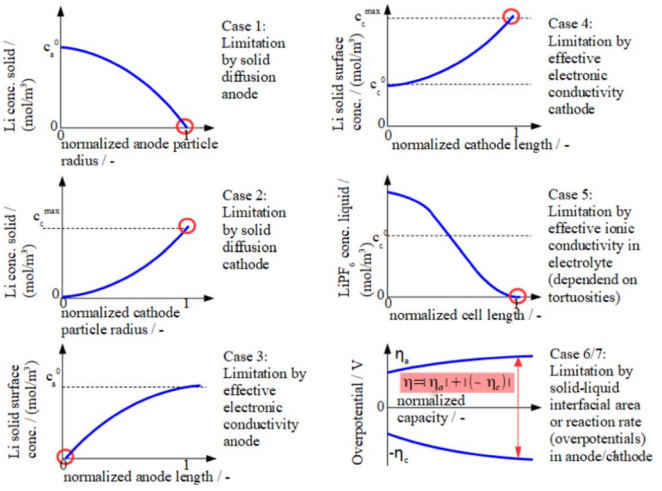

Figure 2. Seven different mechanisms of kinetic performance limitation during discharge which can be analyzed and identified with the aid of a P2D physico-chemical battery model for individual cells.

Results and Discussion

The evaluation of this study consists of three parts. First, results of the two strategies of parameterization will be compared to each other for the case of calendering impact (Assessment of numerical parameterization subsection). As physico-chemical battery models contain about 20 parameters with some of them being hard to determine reliably, deviations between experimental and computational param-

eterization approaches are expected and need to be analyzed. Second, model re-parameterization and the methodology of simulation-supported cell diagnosis will be applied to investigate impacts of further manufacturing parameter variations, being electrode thickness, carbon black content and change of cathode active material. Third, the parameter sets of the various electrode configurations will be statistically analyzed to identify parameter variances and eventually outliers.

Assessment of numerical parameterization.—A parameter set has previously been determined mainly by experiments and literature research[1] for a cell with a non-calendered NMC cathode. It is referred to as reference parameter set in the following. For the same cell the optimization algorithm of Optimization algorithm section was applied and the resulting parameters are listed in Table I together with the reference set. Within the table also the bounds of the particular parameters are listed which were used by the optimization algorithm. In general these intervals were chosen as wide as possible in order to avoid optimal parameter sets which are only based on local minima. However in some individual cases where too large or too small parameter factors would have led to physically unrealistic states, the intervals were chosen restrictively smaller. For the anode lithium start concentration factors were restricted to allow fitting to values higher than the maximum concentration. Furthermore for all concentrations, particle sizes and geometrical electrode parameters the intervals were restricted as well due to the assumption that for these quantities values beyond $\pm$ 50% of their reference value would tend to be more or less physically unrealistic. For tortuosities the lower bounds were restricted to 0.667, respectively, as smaller factors would imply tortuosities smaller than 1 was not reasonable. In general the parameters used for simulation can be divided into two groups. The first contains the initial concentrations c_a^0, c_a^0 and the geometric parameters, being particle radii R_a, R_c, electrode thicknesses δ_a, δ_c and solid volume fractions ε_a, ε_c. These have in common that they can be determined quite accurately which is reflected by their small deviations of up to about $\pm$ 20% from the reference parameters. In the case of the geometric quantities as electrode thicknesses and porosities, these observed deviations may be attributed to production tolerance ranges and measurement uncertainties. As measurements of thickness and porosity often have uncertainties the accuracy of the mathematically identified parameters is seen as being of high quality. The same holds for production tolerances which lead to another source of deviation. The value of $\pm$ 20% can be seen as a range with accounts for accumulated deviation of both, measurement uncertainties and production tolerances. For the particle radii, additionally an error due to the simplifying model assumption of equally sized particles instead of particle size distributions has to be taken into consideration. In the case of initial lithium concentrations, the deviations of parameter fitting can also be seen as realistic due to the assumption of eventual inhomogeneities in SEI layer formation. The second group of parameters contains physico-chemical constants which essentially impact on reaction and transport kinetics and therefore on battery performance at high C-Rates. Diffusion coefficients D_a, D_c, D_e, electronic conductivities σ_a, σ_a, reaction rate coefficients k_a, k_c and tortuosities τ_a, τ_c, τ_s show large deviations between reference and fitting parameters up to some orders of magnitude. This corresponds to the findings of Ecker et al. and Park et al.[11,13] One reason is that these quantities are very hard to determine. Methods like the galvanostatic intermittent titration technique (GITT) which is often used for experimental determination of solid diffusion coefficients,[13] is obviously more complex, time and resource consuming than e.g. the measurement of electrode thickness with the aid of a tactile gauge. The diffusivity is not directly measured but rather derived[23] from other quantities as particle radius and current-voltage-time correlations. Therefore it is doubtful if the attained results really reflect the diffusivity which occurs in a battery cell during discharge. Furthermore it is hard to evaluate if the physico-chemical quantities can be assumed as constant with respect to state of charge and location, i.e. due to lithium concentration gradients within the cell or if certain structural inhomogeneities have to be taken into consideration. The model validation for simulation of the cell with non-calendered NMC cathodes is shown in Figure 3a. The identified parameter set allows to achieve good agreement between experimental and simulated discharge curves for several C-Rates. We hypothetically assume that not only the deviations of discharge capacities at various C-Rates but also the curve shapes are unique for each individual cell and that these characteristics can directly be attributed to the respectively occurring mechanisms of kinetic performance limitation explained in Simulation-supported cell diagnosis section. This becomes obvious especially when comparing the discharge curves at C-Rates $<$ 2C in Figure 3 with the one at 2C. The curves at lower C-Rates show an s-shape, whereas the curve at 2C proceeds rather l-shaped. Figure 3b which depicts the lithium transport shows that for 0.5C and 1C, a limitation by poor electronic conductivity in the cathode causes the reduced discharge capacities with respect to 0.2C in Figure 3a. However, at 2C the maximum lithium concentration in the cathode is quite far away from being reached which reveals that in this case the main limitation at the end of discharge arises not from poor electronic conductivity.

Table I. Reference parameters, bounds used for numerical determination and reparameterised values after fitting for mean value of C-Rate performances among four cells with non-calendered NMC cathodes containing 4% carbon black at a carbon black to binder ratio of 1.

parameter	reference parameter[1]	bounds used to numerical identification	mathematically derived parameter
lithium start concentration in solid (anode) $c_a^0(t=t_0)$/mol m^{-3}	$c_a^0 = 25459$	[0.9; 1.12]	$1.0051c_a^0$
lithium start concentration in solid (cathode) $c_c^0(t=t_0)$/mol m^{-3}	$c_c^0 = 22379$	[0.5; 1.3]	$0.8869c_c^0$
particle radius anode R_a/µm	$R_a = 6.825$	[0.5; 1.5]	$1.1080R_a$
particle radius cathode R_c/µm	$R_c = 6.40$	[0.5; 1.5]	$0.9601R_c$
electrode thickness anode δ_a/µm	$\delta_a = 43.10$	[0.5; 1.5]	$1.0656\delta_a$
electrode thickness cathode δ_c/µm	$\delta_c = 61.36$	[0.5; 1.5]	$1.2150\delta_c$
solid volume fraction anode ε_a^s/-	$\varepsilon_a^s = 0.3871$	[0.9; 1.125]	$0.9000\varepsilon_a^s$
solid volume fraction cathode ε_c^s/-	$\varepsilon_c^s = 0.3040$	[0.9; 1.125]	$0.92018\varepsilon_c^s$
solid diffusion coefficient anode D_a^s/m^2 s^{-1}	$D_a^s = 9.12 \cdot 10^{-15}$	[0.01; 100]	$0.6846D_a^s$
solid diffusion coefficient cathode D_c^s/m^2 s^{-1}	$D_c^s = 3.0 \cdot 10^{-15}$	[0.01; 100]	$1.4851D_c^s$
liquid diffusion coefficient electrolyte D_e/m^2 s^{-1}	$D_e = 0.6832 \cdot 10^{-10}$	[0.01; 100]	$14.9218D_e$
electronic conductivity anode σ_a/S m^{-1}	$\sigma_a = 0.4526$	[0.01; 100]	$0.0138\sigma_a$
electronic conductivity cathode σ_c/S m^{-1}	$\sigma_c = 0.0017$	[0.01; 100]	$1.1918\sigma_c$
reaction rate constant anode k_a/m$^{2.5}$ mol$^{-0.5}$ s^{-1}	$k_a = 2 \cdot 10^{-11}$	[0.01; 100]	$13.593k_a$
reaction rate constant cathode k_c/m$^{2.5}$ mol$^{-0.5}$ s^{-1}	$k_c = 2 \cdot 10^{-11}$	[0.01; 100]	$9.8475k_c$
tortuosity anode τ_a/-	$\tau_a = 1.5$	[0.667; 100]	$17.8109\tau_a$
tortuosity cathode τ_c/-	$\tau_c = 1.5$	[0.667; 100]	$17.8321\tau_c$
tortuosity separator τ_s/-	$\tau_s = 1.5$	[0.667; 100]	$17.9311\tau_s$

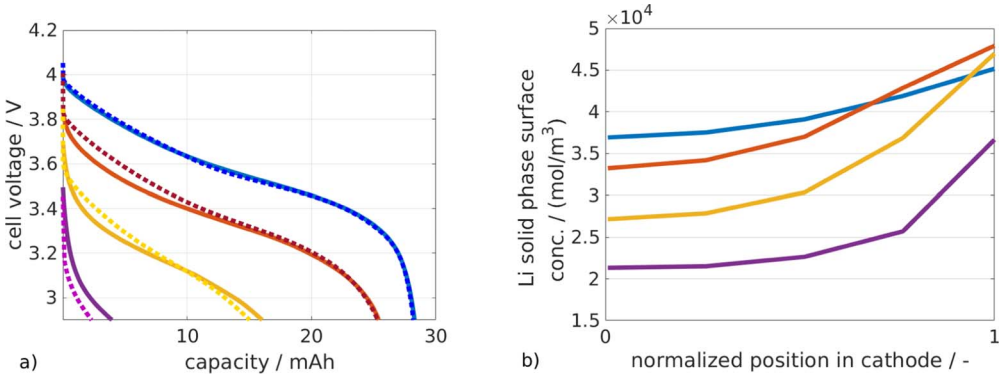

Figure 3. a) Experimental C-Rate curves (dotted lines) and simulated ones (solid lines) after parameterization, for the mean out of four identically manufactured cells with non-calendered NMC cathodes, low carbon black content and carbon black to binder ratio = 1; b) concentrations of Li in solid cathode active material at the end of discharge. In both diagrams, results for 0.2C (blue lines), 0.5C (red lines), 1C (yellow lines) and 2C (purple lines) are shown.

Referring to findings from previous investigations,[1,22] they may rather be caused by a reduction of effective solid-liquid interfacial area leading to high potential losses due to the electrochemical reaction kinetics at higher C-Rates. There are three aspects why the here shown results are interesting. First, in spite of deviations between the reference parameter set and the fitted one, both simulations agree concerning the kinetic performance limitation by poor electronic conductivity at 1C which enhances the reliability that also the faster numerical parameterization approach is able to correctly identify the dominant limitating process. Second, the results presented in this study reveal an interesting add-on to the previous findings[1] where investigations were limited to 1C discharge. Taking additionally discharge at 2C into consideration, shows that the dominant mechanism of limitation changes from electronic conductivity to presumably cathode reaction overpotential between 1C and 2C. An additional simulation study may prove the assumption of overpotential limitation at 2C but will not be considered within the scope of this investigation. Third, the shape of discharge curves seems to be affected by the particular limitation mechanisms. This finding can be helpful for the general interpretation of experimental C-Rate tests and error detection as well.

Impact of calendering stress load.—To investigate how performance and the limiting processes are affected by calendering, in the next step the model was reparameterized to simulate the cell with 22% calendered cathodes at various C-Rates. All further identified parameter sets will be depicted as multiplication factors (as shown in Table AI in the appendix) with respect to the reference parameter set at non-calendered cathodes for the sake of better quantification and compatibility of deviations. As electrode thicknesses and solid volume fractions are individual for each cell these parameters were displayed as multiplication factors of the measured and recalculated values for each parameter configuration in the reference set. The identified factors for the 22 % calendered case show, similarly to the non-calendered case rather small deviations among the first group of geometric and concentration parameters and larger deviations among the second group of kinetic parameters, which are hard to determine experimentally. The essential improvement of the 22 % calendered cathode is an increase of electronic conductivity σ_c which was the dominant deteriorating impact on performance for non-calendered cathodes at 1C. This result corresponds to previous investigations.[1] In the 22 % calendered case, the parameter identification algorithm achieves very good agreement between simulation and real cell behavior as well, as depicted in Figure 4a. Compared to the non-calendered case the performance is significantly improved which is reflected not only by the higher capacities obtained in the discharge curves, but also the cathodic solid lithium concentrations (see Figure 4b) at the end of discharge show that the performance limiting concentration gradients along normalized cell length caused by poor electronic conductivity have significantly decreased. Even at 5C where kinetic losses are highest. The impact of electronic conductivity stays rather small.

Impact of electrode thickness.—A crucial manufacturing parameter variation in battery production plants is the adjustment of electrode thickness. E.g. to change from batteries for high power to high energy applications, the fraction of active material mass in a battery has to be increased. This is often realized by increasing electrode thickness. To analyze the impact of electrode thickness with respect to the cell internal processes of kinetic limitation the thickness of the electrodes was increased for the anode to $\delta_a = 54.78$ µm and for the 22 % calendered NMC cathode to $\delta_c = 61.49$ µm. The corresponding solid

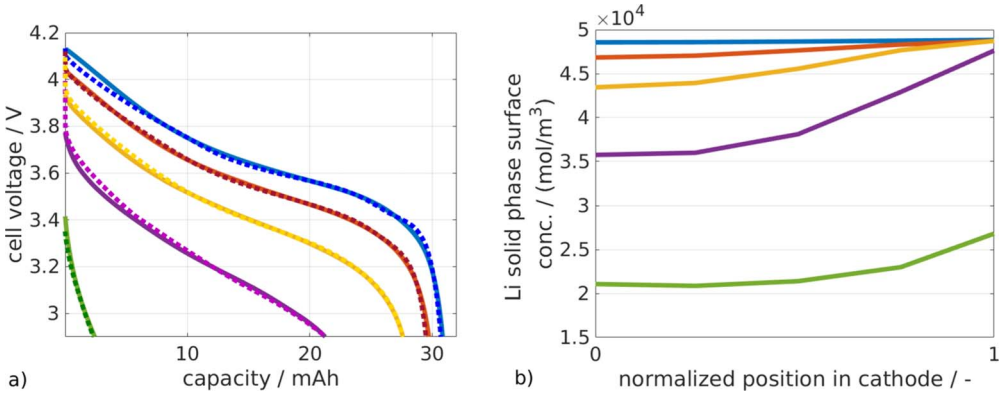

Figure 4. a) Experimental C-Rate curves (dotted lines) and simulated ones (solid lines) based on 18 parameter fitting, for cells with 22% calendered NMC cathodes, low carbon black content and carbon black to binder ratio = 1; b) concentrations of Li in solid cathode active material at the end of discharge. In both diagrams results for 0.2C (blue lines), 0.5C (red lines), 1C (yellow lines), 2C (purple lines) and 5C (green lines) are shown.

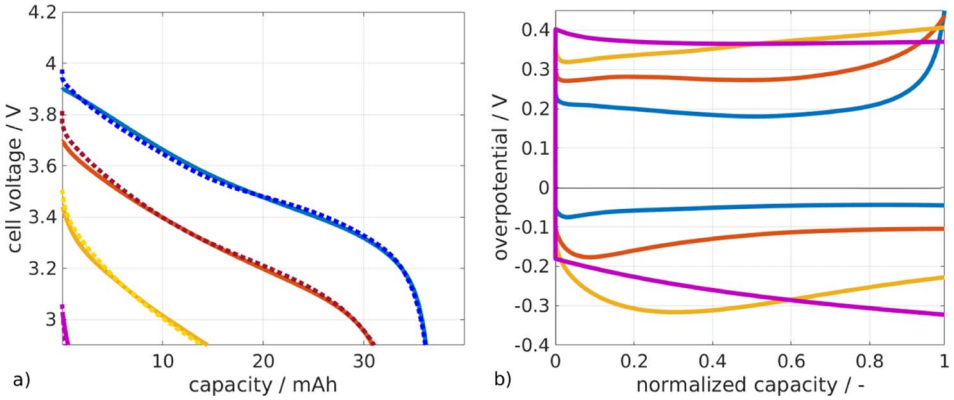

Figure 5. a) Agreement between experimental C-Rate curves (dotted lines) and simulated ones (solid lines) for cells with increased electrode thickness, 22% calendered NMC cathodes, low carbon black content and carbon black to binder ratio = 1; b) overpotentials arising during discharge in the cathode. In both diagrams results for 0.2C (blue lines), 0.5C (red lines), 1C (yellow lines) and 2C (purple lines) are shown.

volume fractions were calculated. For all other parameters, values of the reference set were taken as initial values for the identification algorithm. Results are displayed in Figure 5 and Table AI. The experimental and simulated discharge curves in Figure 5a show very good agreement. The discharge capacity at 0.2C is approximately 10 % higher than that of the previously discussed curve high which is attributed to the increased active material volume. However, already at 0.5C a reduction of discharge capacity by about 15 % can be observed. At 1C, the reduction amounts to almost 60 % and at 2C almost no capacity can be reached by the cell. Compared to the thin cells depicted in Figure 4a, the cell with increased electrode thicknesses thus performs significantly worse, especially at higher C-Rates. Analysis of the limitation mechanisms suggests that the losses of the thicker electrodes were mainly caused by overpotentials which are depicted in Figure 5b. At 0.2C the anode overpotential is dominant with 0.2 V and increases significantly at the end of discharge. At higher C-rates these overpotentials increase toward 0.4 V. The strongly exponential course at the end of the discharge (normalized capacitance approaching 1) is not of central importance as it only reflects the reaching of the lower voltage limit and thus the sudden drop of the cell voltage. Decisive for the interpretation of the overpotential curves are the absolute values which occur during the actual discharge (normalized capacity in the range from >0 to about 0.9), because these represent purely kinetic performance losses which could possibly be reduced by adjusting manufacturing parameters. Towards higher C-rates it can be observed in Figure 4b that also the overvoltages in the cathode reach absolute values of about 0.3 V. The total overpotential sums up with the anode-side approximately 0.4 V to almost 0.7 V, which then reflects the performance loss as cell voltage drop in the discharge characteristics. It is assumed that limitations by overpotentials in the porous electrodes of LIB arise from an effectively decreased solid-liquid interfacial area which are caused by insufficient mixing or contacting of components, e.g. inhomogeneities of carbon black binder matrix or by general lack in components, e.g. too low carbon black content.[22] These deficiencies may result in particular fractions of the interfacial area which are not sufficiently supplied with electrons and therefore become cut off from the electrochemical reaction. At first, this does not seem to be characteristic for the influence of the layer thickness. We assume, however, that in this case it is not the direct effects of the layer thickness increase, such as longer transport distances for lithium and electrons, that trigger the performance loss, but that reaction kinetically unfavorable side effects of the layer thickness increase are involved. These could be, for example, segregation effects or dehomogenization of the electrode structure or material composition due to an increased temperature gradient during solvent evaporation during electrode drying. Westphal et al. have shown that an increase in layer thickness increases the segregation of the inactive material[24] which supports the result of the simulation.

Impact of carbon black content and CB:B ratio.—As shown in previous work,[1] poor performance of cells which suffer from low electronic conductivity may be enhanced by increasing the carbon black (CB) content and the carbon black to binder ratio. This should aim to prevent electronically conductive pathways from becoming isolated by an entire covering of particles by the non-conductive binder.[21,22] To distinguish between different possible limitations, in these studies the CB amount was increased to an extent which lets us assume that there is no limitation due to low electronic conductivity. Comparing the discharge curves (see Figure 6a with the ones depicted in previous sections (Assessment of numerical parameterization, Impact of calendering stress load and Impact of electrode thickness) shows that the cell performed significantly better after increasing the cathodic carbon black content from 4 to 5.88 mass-% and simultaneously the carbon black to binder ratio from CB:B = 1 to CB:B = 1.5. Up to 2C, the discharge curves lie closely together and almost reach the theoretical capacity of 1.40 mAh cm^{-2} · 24.95 cm^2 = 34.93 mAh. This improvement is achieved as limitations by poor electronic conductivity and overpotentials in the cathode could be reduced. Only at 5C the discharge capacity was significantly deteriorated. Modelling results suggest that instead of electronic conductivity the most limiting process

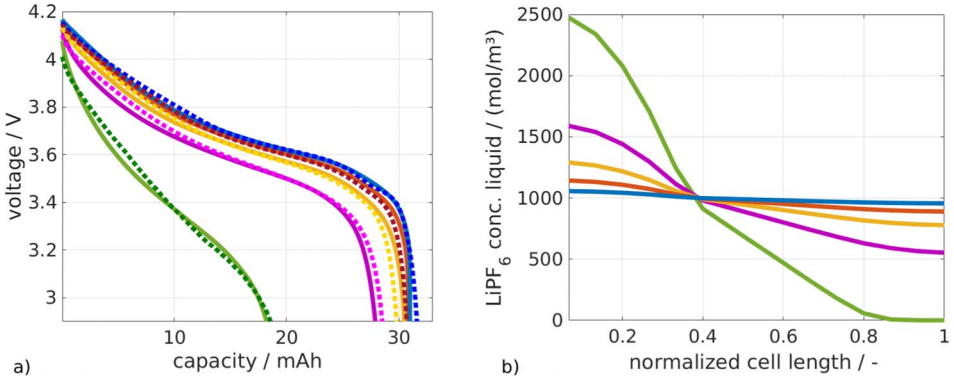

Figure 6. a) C-Rate curves (dotted lines) and simulated ones (solid lines) based on computational parameter determination, for cells with increased carbon black content (5.88 %) and carbon black to binder ratio (CB:B = 1.5) where thin, 22% calendered NMC cathodes were used; b) concentrations of $LiPF_6$ in the electrolyte at the end of discharge. In both diagrams results for 0.2C (blue lines), 0.5C (red lines), 1C (yellow lines), 2C (purple lines) and 5C (green lines) are shown.

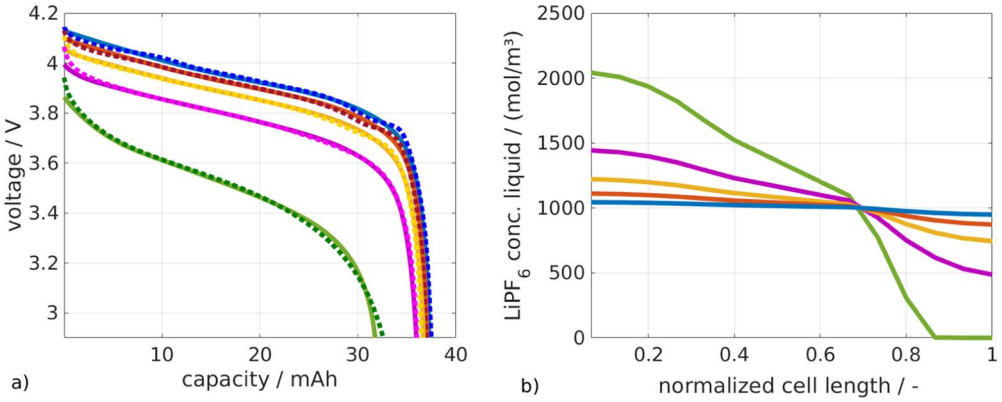

Figure 7. a) Agreement between experimental C-Rate curves (dotted lines) and simulated ones (solid lines) based on parameter fitting, for cells containing 30% calendered LMO cathodes with increased carbon black content (5.88 %), carbon black to binder ratio (CB:B = 1.5) and increased thickness and b) concentrations of $LiPF_6$ in the electrolyte at the end of discharge. In both diagrams results for 0.2C (orange lines), 0.5C (red lines), 1C (green lines), 2C (blue lines) and 5C (pink lines) are shown.

has been changed to effective ionic conductivity of $LiPF_6$ in the electrolyte which, however, only cause significant performance losses at C-rates higher than 2C. This is visible in the depletion of lithium at the end of 5C discharge close to the current collector (see Figure 6b). The concentration curve at 5C also reflects the relatively high contribution by anode tortuosity which yields $\tau_a = 5.73$, i.e. a 3.8162 times higher value (see Table AI in the appendix). The contribution can be observed as the $LiPF_6$ gradient is especially high along the anode (normalized cell length 0 to about 0.36). For separator and cathode (normalized cell length > 0.36), the gradient is lower which corresponds to the smaller increases by about $1.6655\tau_s$ and $1.1169\tau_c$ times (see Table AI). As stated previously, also the shape of discharge curves is particular for different limitation processes. Here it seems to be characteristic for limitation by ionic conductivity that an unproportionally large gap emerges between the C-Rates where the limitation becomes dominant, in this case between 2C and 5C. For comparison, the distances between the discharge curves which were shown in Assessment of numerical parameterization – Impact of electrode thickness sections where limitations by electronic conductivity or overpotentials were dominant, are rather equidistant or (in the case of 22 % calendered cathodes with low carbon black content and $\delta_c = 48.95$ µm in Impact of calendering stress load section) at least proportionally increasing.

Impact of cathode material.—In the development of LIB, the choice of cathode material is crucial. Different than in the case of anodes where usually graphite is used and options are relatively limited, cathode materials are usually mixed compositions which contain in many cases problematic materials such as e.g. cobalt. Replacement of Co by non-toxic and abundant materials like manganese usually leads to performance losses, e.g. in energy density. In general substitution of old and development of new cathode material appears to be a relevant concern in battery productions. In the scope of this work, the simulation was exemplary applied to a change of cathode materials, from NMC to LMO. Despite of the adjustment of LMO related polynomial of open circuit potential, the agreement between simulation after parameter fitting and corresponding experimental discharges is very good (see Figure 7a). Similar to the best performing NMC cell, the discharge curves of cells containing LMO cathodes show only small performance losses up to 2C and an unproportional deterioration between 2C and 5C. Figure 7b depicts the concentration of $LiPF_6$ in the electrolyte at the end of discharge for the various C-Rates. It confirms the assumption of a characteristic indicator for limitation by poor ionic conductivity as the corresponding concentration at 5C drops to zero mol/m^3 at the border location between cathode and current collector (normalized cell length ≈ 0.85).

Computational parameter identification.—A useful side product of reparameterization for various cell configurations is that each particular parameter becomes identified several times, which increases statistical certainty. Variance ranges and eventual outliers can be derived. Within the scope of this work, five parameter sets were derived and the reference parameter set was additionally taken into consideration as a sixth set for statistical evaluation. Based on the fitting factors, boxplots were developed (see Figure 8). The central mark in each box represents the median and 25th and 75th percentiles are indicated by the bottom and top edges, respectively. The whiskers reach to the values which deviate most from median but are no outliers. The outliers are depicted by red crosses. The boxplots were derived for the two parameter groups, respectively, which were categorized in previous sections according to their uncertainty and identifiability. The first group includes parameters which can be measured directly and deviations are found to be relatively small, as depicted in Figure 8a. The electrode thicknesses and solid volume fractions show overall reasonable deviations of about 10 % which can be attributed to production and measurement uncertainties. Only the deviations of δ_c seem to be a bit too high which may be caused by enhanced thickness inhomogeneities among non-calendered cathodes.[21] Deviations from

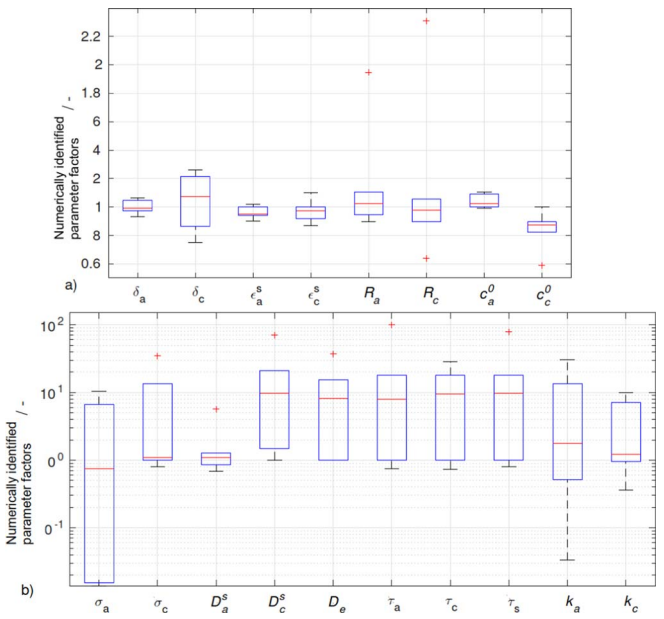

Figure 8. Box plot analysis of a) identified geometry and concentration parameters with relatively small deviations and b) identified kinetic parameters and tortuosities which show relatively large deviation ranges.

the targeted thickness due to coating uncertainty and measurement inaccuracy can be sources of errors. Both together are estimated to accumulate to realistic deviations of 20 %. E.g. for the cathode used in the reference configuration this would yield δ_c=48.95+/−0.979 µm. The material densities for calculation of solid volume fractions were taken from literature[25–27] and may deviate in reality, especially for the active cathode materials which are mixtures of several elements causing uncertainties for density determination. Furthermore the equation also depends on the measured electrode mass loading which is assumed to have an uncertainty of about 2 %. Concerning the particle radii, the boxplots and associated deviations are rather small. The P2D physico-chemical model does not cover in reality occurring particle size distributions. It confirms the findings of Röder et al.[28] that impacts of particle size distributions are significant and may be underrepresented in conventional models. Therefore the model will identify values for averaged particle radii which represent experimentally observed behavior best. The model-based study shows that only in certain cases of distributions and currents, a lumped mean particle size produces similar results as a distribution. However, as many parameters have such a distribution, enlarging the model for all distributions would render it extremely complex to solve. Furthermore distributions are often not quantitatively and precisely measurable. In three cases outliers could be identified which may particularly attributed by the averaged particle sizes in the model. However, this issue may also have other reasons, e.g. an overlapping impact of particle size and solid diffusion constant. The effects of these two quantities have to be assumed as being quite similar. A possibly resulting non-uniqueness between both parameters has to be investigated in future studies. The deviations of initial lithium concentrations c_0 in anode and cathode are below 20 % and for the reference parameter set they were calculated by Faraday's law at low C-Rates:

$$c_0 = \frac{C}{F \cdot \varepsilon_{act}^s \cdot V} \quad [8]$$

The c_0-values in the model are based on the amount of Li which was shifted between the electrodes on the electrode volume V before the C-Rate started, i.e. during formation. Uncertainties in this calculation arise due to losses of lithium during formation which are a result of SEI layer growth[29] and eventually other side reactions which we assume to be not exactly identifiable. Therefore the magnitude of concentration deviations among the parameter sets shown in Figure 8a appear realistic to us, even the statistical outlier at about $0.6c_c^0$ does not necessarily has to be unrealistic from physical point of view as the extent of SEI inhomogeneities and side reactions can hardly be quantified and may fluctuate especially for non-commercial cells. Previous investigations[1,22] revealed that effective electronic conductivities of the porous electrodes are very sensitive to manufacturing impacts and may in the worst case behave like a loose connection with high electric resistances. As a consequence, high deviations of several orders of magnitude[11] are reflected in literature among the studies about determination of effective electronic conductivity. The diffusion coefficients of lithium within the active material can be derived experimentally, e.g. by GITT or PITT[11,23] which is quite extensive, though. Furthermore the review of Park et al.[13] shows that high variations of several orders of magnitude for diffusion coefficients are presented in the studies of different authors, even among similar active materials. Therefore the particularly high deviations which can be observed in Figure 8b for the diffusion coefficients D_a^s and D_c^s are assumed to be reasonable and may be attributed to inhomogeneities across the electrode or due to concentration dependence. The high deviation for the liquid diffusion coefficient D_e is rather unexpected. Similar as mentioned above for particle radius and solid diffusion coefficient, for the ionic transport in the liquid an overlapping of impacts of tortuosity and liquid diffusion coefficient cannot be excluded. However, this does not change the significance of the simulative identification of the limitation by ionic transport within the context of the seven mechanisms of limitation which were discussed in Simulation-supported cell diagnosis section. The tortuosities of anode, cathode and separator are determined by the respective pore structures and denote the effective transportation lengths of $LiPF_6$ within the electrolyte. In the physico-chemical model the tortuosity is implemented as a dimensionless quantity which corresponds to the quotient of effective transportation length and thickness of anode, cathode or separator, respectively. Therefore a tortuosity ≤ 1 is physically not reasonable. In electrodes for lithium-ion-batteries tortuosity depends on the porosity and range about 1.2-4.0.[30] However, Thorat et al.[14] also refer to sources which presented tortuosities up to 27 which elucidates that this parameter is also subject to certain variances. The results from parameter fitting show even stronger fluctuations. The factors shown in Figure 8b, multiplied with the reference tortuosity of $\tau = 1.5$, yield a range of tortuosities from 1.1 to 42.9, taking the outliers into consideration even up to 149.8. This appears quite inaccurate but the simulations shows that even high deviations are not necessarily responsible for performance limitations. In the cases of NMC cathodes with low carbon black content and CB:B = 1, relatively high tortuosities were calculated but they are still not crucial as performance limitation is dominated by poor electronic conductivities and overpotentials. However, for cathodes with high carbon black content and CB:B = 1.5 where these limiting factors were eliminated, tortuosities only slightly larger than one become a sensitive contributor. This implies that if the cell performance is limited by other processes, e.g. electronic conductivity at lower C-Rates already, the model is insensitive to tortuosity and tortuosity identification is barely possible. In general the results show that the model does not enable to identify all parameters by mathematical determination as non-limiting processes in a particular battery cell cause that the respectively concerned parameters may become insensitive resulting in unrealistically high deviations. In this context the relatively high deviations of reaction rate constants have to be pointed out as well. The reaction rate constant seems to be even more difficult to determine experimentally than diffusion coefficients as corresponding investigations are scarce to find in literature. However, the fact that this quantity is assumed to be effectively influenced by solid-liquid interfacial area and by the structure of the carbon black binder matrix in a wider sense, elucidates its likeliness to fluctuate significantly.

Relevance of limitation analysis in battery production.—From the previous sections it can be stated that in spite of non-identifiability of non-limiting parameters, the model seems to be able to predict limiting processes from a set of discharge curves. Furthermore, the values of the respectively limiting parameters determined by the model appear to be realistic and can therefore help to gain knowledge about these quantities. The combination of fast reparameterization and the model ability to identify limiting processes of particular cells at different C-Rates can be incorporated in industrial applications for error detection during development and production of battery cells and optimization of manufacturing parameters as depicted within the scheme in Figure 9. E.g. aiming to use the cell with high carbon black content discussed in Impact of carbon black content and CB:B ratio section for application in electric vehicles may require to improve the cell performance at 5C which is significantly worse than for lower C-Rates. Whereas experimental test of cell performance only detects the malfunction but not the reason of failure, the model allows to identify the limiting process which in this case would be the ionic transport out of the seven processes presented in Figure 2, at 5C for the particular cell. With the knowledge of the limiting process, the manufacturing parameters for optimization can be narrowed down. First it becomes explicit if the performance losses at 5C arise in the anode, cathode or in the electrolyte which already simplifies the error detection significantly. Second it can be evaluated which particular parameters should be improved. E.g. in the case of electrolytic limitation it has to be further analyzed with the model if tortuosity is responsible for performance losses or ionic conductivity of the electrolyte. Tortuosity limitation could be reduced by increasing porosity or eventually also by reduction of binder content which as an inactive solid component may have an effect of blocking channels to be filled up with electrolyte. In case of the ionic conductivity limitation another electrolyte recipe is most probable to improve cell performance. In general it is

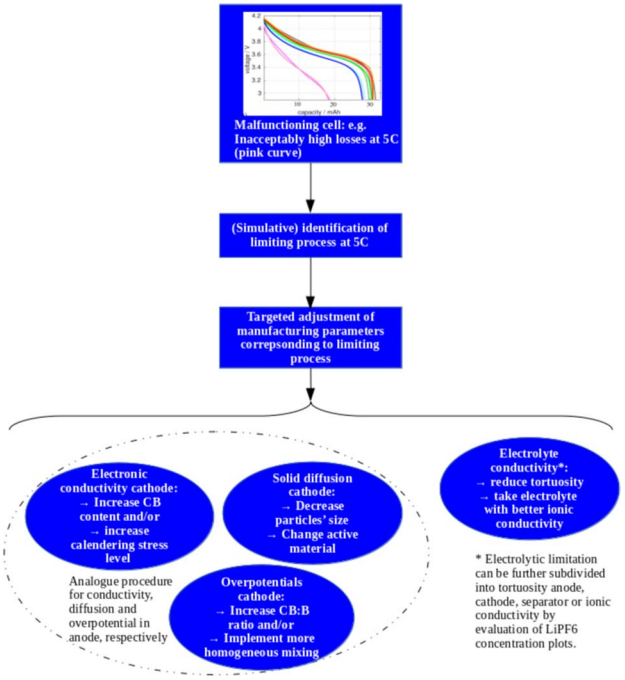

Figure 9. Scheme of error detection and targeted optimization of manufacturing parameters with the aid of simulative limitation process identification.

recommended for further research to implement this simulation-supported methodology into a battery production plant to test its efficiency in practical use.

Conclusions

Battery cells with various configurations of calendering stress loads, electrode thicknesses, carbon black recipes and cathode active materials were analyzed. A physico-chemical model with reference parameters from previous work was reparameterized for all cell configurations with the goal to simplify model parameterization by solely applying mathematical identification using a set of discharge curves. This allows fast identification of the cell internal performance limitations, respectively. As the model enables to identify the most limiting out of seven cell internal processes, it constitutes a powerful complementary tool to measurement based diagnostics for failure detection in battery production plants. The method of simulative identification of limiting processes was tested for a reference cell and four other impacts implemented by the manufacturing parameter variations. In spite of deviations between parameter sets developed experimentally and by mathematical parameter identification from discharge curves, the dominant limitating factor of poor electronic conductivity in the reference cells containing non-calendered cathodes could be confirmed. Additionally, it was shown that also overpotentials which are assumed to be caused by limitations of electrochemically active solid-liquid interfacial area, cause significant performance limitations, even for a calendering level of 22 % volume reduction. This impact is even amplified when the electrode thickness increases and it is probable that a higher carbon black content a higher carbon black to binder ratio is necessary to reduce these overpotentials. Cells with improved electronic conductivity and overpotentials allowed to increase cell performance. However, the cells still showed an unproportionally high performance deterioration between 2C and 5C which was shown to be a characteristic indicator for limitation by poor ionic conductivity. This limitation was observed similarly for NMC and LMO, where the models open circuit potential was adjusted to reproduce the LMO-typical discharge behavior. Finally, the various parameter sets were analyzed regarding deviations among the particular parameters as a computational contribution to the state of knowledge about parameter identification which commonly is performed by extensive experimental approaches.

Acknowledgement

Thanks for financial funding to the German Federal Ministry of Education and Research. Thanks for technical support to the Institute for Particle Technology and to the Institute of Environmental and Sustainable Chemistry, both TU Braunschweig.

Appendix A:

Table AI. Parameter sets determined by fitting the simulation to C-Rate performances of cells with various manufacturing impacts.

parameter	cell a: NMC, 22% calendered, CB = 4%, CB:B = 1, thin δ	cell b: NMC, 22% calendered, CB = 4%, CB:B = 1, increased δ	cell c: NMC, 22% calendered, CB = 5.88%, CB:B>1, thin δ	cell d: LMO, 30% calendered, CB = 5.88%, CB:B>1, increased δ
lithium start concentration in solid (anode) $c_a^0(t=t_0)$/mol m^{-3}	$1.0944c_a^0$	$1.1059c_a^0$	$1.0395c_a^0$	$0.9917c_a^0$
lithium start concentration in solid (cathode) $c_c^0(t=t_0)$/mol m^{-3}	$0.8596c_c^0$	$0.8244c_c^0$	$0.8982c_c^0$	$0.5897c_c^0$
particle radius anode R_a/μm	$0.8976R_a$	$1.9463R_a$	$1.0478R_a$	$0.9482R_a$
particle radius cathode R_c/μm	$0.8977R_c$	$2.3093R_c$	$0.6405R_c$	$1.4885R_c$
electrode thickness anode δ_a/μm	$0.9893\delta_a$	$0.9354\delta_a$	$1.0448\delta_a$	$0.9756\delta_a$
electrode thickness cathode δ_c/μm	$0.7501\delta_c$	$1.2635\delta_c$	$0.8663\delta_c$	$1.1493\delta_c$
solid volume fraction anode ε_a^s/-	$0.9502\varepsilon_a^s$	$0.9414\varepsilon_a^s$	$1.0198\varepsilon_a^s$	$0.9501\varepsilon_a^s$
solid volume fraction cathode ε_c^s/-	$1.1008\varepsilon_c^s$	$0.8706\varepsilon_c^s$	$0.9541\varepsilon_c^s$	$0.9962\varepsilon_c^s$
solid diffusion coefficient anode D_a^s/m^2 s^{-1}	$0.8578D_a^s$	$1.2696D_a^s$	$1.2008D_a^s$	$5.6942D_a^s$
solid diffusion coefficient cathode D_c^s/m^2 s^{-1}	$12.9912D_c^s$	$20.8939D_c^s$	$6.6224D_c^s$	$70.0629D_c^s$
liquid diffusion coefficient electrolyte D_e/m^2 s^{-1}	$15.3240D_e$	$36.9364D_e$	$1.2625D_e$	$1.0000D_e$
electronic conductivity anode σ_a/S m^{-1}	$0.0153\sigma_a$	$10.3541\sigma_a$	$6.5996\sigma_a$	$0.5000\sigma_a$
electronic conductivity cathode σ_c/S m^{-1}	$1.8633\sigma_c$	$1.8633\sigma_c$	$13.5569\sigma_c$	$34.7155\sigma_c$
reaction rate constant anode k_a/m$^{2.5}$ mol$^{-0.5}$ s^{-1}	$0.5091k_a$	$0.0331k_a$	$30.5065k_a$	$2.5577k_a$
reaction rate constant cathode k_c/m$^{2.5}$ mol$^{-0.5}$ s^{-1}	$0.9597k_c$	$0.3623k_c$	$7.0542k_c$	$1.4141k_c$
tortuosity anode τ_a/-	$12.2598\tau_a$	$99.8386\tau_a$	$3.8162\tau_a$	$0.7446\tau_a$
tortuosity cathode τ_c/-	$17.9994\tau_c$	$28.6097\tau_c$	$1.1169\tau_c$	$0.7402\tau_c$
tortuosity separator τ_s/-	$17.9994\tau_s$	$78.3007\tau_s$	$1.6655\tau_s$	$0.8030\tau_s$

List of Symbols

A	geometric area, m^2
a_{sl}	solid-liquid interfacial area, $m^2\ m^{-3}$
α	transfer coefficient, -
c	concentration, mol m^{-3},
C	capacity, Ah,
δ	electrode thickness, m
D	diffusion coefficient, $m^2\ s^{-1}$
ε	volume fraction (porosity), -
ε_s	volume fraction of solid component, -
F	Faraday's constant, 96485 C mol^{-1}
I	current, A
j^{Li}	volume rate of Li^+ current generation A m^{-3}
j_0	exchange current density A m^{-2}
J	current density A m^{-2}
κ	ionic conductivity S m^{-1}
k	reaction rate constant, $m^{2.5}\ mol^{-0.5}\ s^{-1}$
L	length, m
M	molar mass, g mol^{-1}
n	amount of substance, mol
η	overpotential, V
r	radial coordinate, -
R	ideal gas constant, 8.314 J $mol^{-1}\ K^{-1}$
R_p	particle radius, m
ρ	density, g m^3
t_+	Li^+ transference number, -
σ	electronic conductivity, S m^{-1}
SOC	state of charge, -
τ	tortuosity, -
T	temperature, K
U	open circuit potential, V
V	volume, m^3
ϕ	electric potential, V
ϖ	electrode material loading, g m^{-2}
x	spacial coordinate
ζ	mass fraction, -

Superscripts and Subscripts

a	anode
c	cathode
cal	calendered
DL	double layer
e	electrolyte
eff	effective
Li	Lithium
max	maximum
s	solid
0	initial

ORCID

Georg Lenze https://orcid.org/0000-0001-6649-8225
Ulrike Krewer https://orcid.org/0000-0002-5984-5935

References

1. G. Lenze, F. Röder, H. Bockholt, W. Haselrieder, A. Kwade, and U. Krewer, *Journal of The Electrochemical Society*, **164**(6), A1223 (2017).
2. A. A. Tahmasbi, T. Kadyk, and M. H. Eikerling, *Journal of The Electrochemical Society*, **164**(6), A1307 (2017).
3. A. A. Tahmasbi and M. H. Eikerling, *Electrochimica Acta*, **283**, 75 (2018).
4. A. Bielefeld, D. A. Weber, and J. Janek, *The Journal of Physical Chemistry C*, **123**(3), 1626 (2019).
5. R. Koerver, W. Zhang, L. de Biasi, S. Schweidler, A. Kondrakov, S. Kolling, T. Brezesinski, P. Hartmann, W. G. Zeier, and J. Janek, *Energy and Environmental Science*, **11**(8), 2142 (2018).
6. E. Martinez-Rosas, R. Vasquez-Medrano, and A. Flores-Tlacuahuac, *Computers and Chemical Engineering*, **35**, 1937 (2011).
7. N. Legrand, S. Raël, B. Knosp, M. Hinaje, P. Desprez, and F. Lapicque, *Journal of Power Sources*, **251**, 370 (2014).
8. A. M. Colclasure and R. J. Kee, *Electrochimica Acta*, **55**, 8960 (2010).
9. M. Torchio, L. Magni, B. Gopaluni, R. D. Braatz, and D. Raimondo, *Journal of The Electrochemical Society*, **163**(7), A1192 (2016).
10. I. D. Campbell, K. Gopalakrishnan, M. Marinescua, M. Torchio, G. J. Offer, and D. Raimondo, *Journal of Energy Storage*, **22**, 228 (2019).
11. M. Ecker, T. K. D. Tran, P. Dechent, S. Käbitz, A. Warnecke, and D. U. Sauer, *Journal of The Electrochemical Society*, **162**(9), A1836 (2015).
12. M. Ecker, S. Käbitz, I. Laresgoiti, and D. U. Sauer, *Journal of The Electrochemical Society*, **162**(9), A1849 (2015).
13. M. Park, X. Zhang, M. Chung, G.B. Less, and A. M. Sastry, *Journal of Power Sources*, **195**, 7904 (2010).
14. I. V. Thorat, D. E. Stephenson, N. A. Zacharias, K. Zaghib, J. N. Harb, and D. R. Wheeler, *Journal of Power Sources*, **188**, 592 (2009).
15. J. Ott, B. Völker, Y. Gan, R. M. McMeeking, and M. Kamlah, *Acta Mechanica Sinica*, **29**(5), 682 (2013).
16. R. Masoudi, T. Uchida, and J. McPhee, *Journal of Power Sources*, **291**, 215 (2015).
17. J. C. Forman, S. J. Moura, J. L. Stein, and H. K. Fathy, *Journal of Power Sources*, **210**, 263 (2012).
18. G. Lenze, N. Lin, and U. Krewer, *ModVal12*, Freiburg, Germany, (2015).
19. U. Krewer, F. Röder, E. Harinath, R. Braatz, B. Bedürftig, and R. Findeisen, *Journal of The Electrochemical Society*, **165**, A3656 (2018).
20. U. Krewer, H.-K. Yoon, and H.-T. Kim, *Journal of Power Sources*, **175**(2), 760 (2008).
21. G. Lenze, H. Bockholt, C. Schilcher, L. Froböse, D. Jansen, U. Krewer, and A. Kwade, *Journal of The Electrochemical Society*, **165**(2), A314 (2018).
22. H. Bockholt, W. Haselrieder, and A. Kwade, *Powder Technology*, **297**, 266 (2016) .
23. S.-M. Lee, S.-Y. Lee, Y.-G. Lee, Y.-M. Lee, H.-K. Park, J.-K. Park, and S.-W. Song, Editor: J.-K. Park, *Principles and Applications of Lithium Secondary Batteries*, p. 238-257, Wiley-VCH (2012).
24. B. Westphal and A. Kwade, *Journal of Energy Storage*, **18**, 509 (2018).
25. H. Yoshizawa and T. Ohzuku, *Journal of Power Sources*, **174**, 813 (2007).
26. W. Haselrieder, S. Ivanov, H. Y. Tran, S. Theil, L. Froböse, B. Westphal, M. Wohlfahrt-Mehrens, and A. Kwade, *Progress in Solid State Chemistry*, **42**, 157 (2014).
27. C. Wurm, O. Öttinger, S. Wittkämper, R. Zauter, and K. Vuorilehto, *Handbuch Lithium-Ionen-Batterien*, p. 49, Springer, Berlin Heidelberg (2013).
28. F. Röder, S. Sonntag, D. Schröder, and U. Krewer, *Energy Technology*, **4**, 1588 (2016).
29. P. Arora and R. E. White, *Journal of The Electrochemical Society*, **145**(10), 3647 (1998) .
30. D.-W. Chung, M. Ebner, D. R. Ely, V. Wood, and R. E. Garcia, *Modelling and Simulation in Materials Science and Engineering*, **21**(7), 074009 (2013).